Global Journal of Pure and Applied Mathematics.
ISSN 0973-1768 Volume 12, Number 4 (2016), pp. 3535-3543

http://www.ripublication.com/gjpam.htm

Investigation Of Dynamic Positioning Of The Electron Beam On The Chemical Composition Of Weld In Electron Beam Welding

Ekaterina S. Salomatova
Junior Research Scientist Perm National Research Polytechnic University, Komsomolskiy prospect, 29, Perm, 614099, Russian Federation

Dmiriy N. Trushnikov
PhD in Technical Sciences, Perm National Research Polytechnic University, Komsomolskiy prospect, 29, Perm, 614099, Russian Federation

Tatiana V. Olshanskaya
PhD in Technical Sciences, Assistant professor, Perm National Research Polytechnic University, Komsomolskiy prospect, 29, Perm, 614099, Russian Federation

Vladimir Ya. Belenkiy
Doctor in Technical Sciences, Professor Perm National Research Polytechnic University, Komsomolskiy prospect, 29, Perm, 614099, Russian Federation

Abstract

The paper describes the numerical model of the processes of evaporation, condensation and diffusion of alloy components 5056 in electron beam welding with a tandem three electron beam, which allows you to predict the chemical composition of the weld. When building the model, we adopted the following the assumptions: the shape of the keyhole is approximated by a cylinder, the surface of the keyhole is considered to be isothermic, heat and mass transfer of material along the keyhole axis are considered insignificant, the diffusion coefficient in the melt depends on temperature, the depletion of alloying elements in the melt takes place in a thin layer on the surface of the keyhole and due to high pressure in the keyhole, the speed of metal vapour at

the outlet reaches the local sonic speed. Thus, the problem reduces to two dimensions and the computational domain contains only the liquid phase. To solve the problem, we can use a numerical method that takes into account the evaporation, condensation and diffusion of elements in the melt. Investigated macrosections sectional passages using X-ray fluorescence analysis, the results of which coincide with the calculated values.

Keywords: electron beam welding, diffusion processes, dynamic positioning electron beam, losses of alloying elements.

Introduction

For decades electron beam welding (EBW) is widely used in automobile, aircraft, space, power, shipbuilding industries and other ones. The facilities of the improvement of EBW technologies occurred with the development of modern methods of electron beam controlling [1], in particular, with the use of oscillation and electron beam dynamic positioning. EBW with electron beam oscillation allows to obtain more homogeneous macro-and microstructure of welded joints [2]. Dynamic positioning of electron beam with the formation of several heat sources provides heat input to specimens in some areas apart from each other [3-5], which allows to product high-quality welded joints from dissimilar materials [6], increase the efficiency of EBW and decrease the porosity of a joint [1].

Physical processes occurring during interaction of electron beam with a metal are complex. At EBW deep and narrow steam-gas channel is formed in the area of interaction of a concentrated electron beam with a metal. The liquid is hold on the channel walls by vapor pressure [7-10]. At EBW with the dynamic positioning of electron beam several steam-gas channels are formed (Fig. 1), where an intensive metal evaporation takes place, which may lead to the depletion of some alloying elements in molten metal. Such process can be observed in metal alloys containing alloying elements having low melting points.

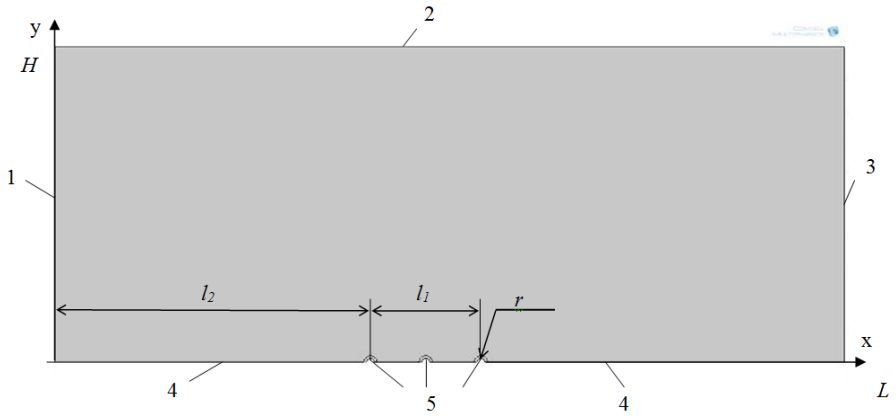

Fig. 1. The calculation scheme. 1-front boundary; 2-lateral boundary; 3-output boundary; 4-an axis of symmetry; 5-keyholes

At present significant progress is achieved in simulating of a welded joint formation process at EBW [11-15] and evaporation processes. Two evaporation mechanisms, connected with concentration and pressure gradients [16], are known, and a theory of the evaporation processes at energy beam welding has been developed [17].
When simulating laser welding, which is close to electron beam processes, the temperature in weld penetration channel is generally accepted to be equal to boiling point at atmospheric pressure, but this assumption is inadmissible when simulating electron beam welding because this process is carried out in vacuum.

Formulation of the problem: defining equation and boundary conditions
When building the model, we adopted the following the assumptions: the shape of the keyhole is approximated by a cylinder, the surface of the keyhole is considered to be isothermic, heat and mass transfer of material along the keyhole axis are considered insignificant, the diffusion coefficient in the melt depends on temperature, the depletion of alloying elements in the melt takes place in a thin layer on the surface of the keyhole and due to high pressure in the keyhole, the speed of metal vapour at the outlet reaches the local sonic speed.
Thus, the problem reduces to two dimensions and the computational domain contains only the liquid phase. To solve the problem, we can use a numerical method that takes into account the evaporation, condensation and diffusion of elements in the melt. The calculation scheme is shown in Fig. 1.
The system of equations describing the processes of evaporation in EBW includes the momentum transport equation (Navier-Stokes):

$$\left(\vec{U}\cdot\nabla\right)\vec{U} = -\frac{\nabla P}{\rho} + \nu\nabla^2\vec{U}, \quad (1)$$

the energy transport equation:

$$\rho c_p\vec{U}\cdot\nabla T = \nabla(\lambda\nabla T), \quad (2)$$

and the impurity transport equation:

$$\vec{U}\cdot\nabla S = D(\nabla^2 S), \quad (3)$$

where Ū-the velocity field of the melt; P-the pressure in the melt, ρ is the melt density, Pa; ν-the kinematic viscosity coefficient, m^2/sec; c_p-the heat capacity at constant pressure J/K; λ-the heat conduction coefficient, V/m·K; S_i-the concentration of component i in the alloy, %; T-the temperature of the keyhole walls, K; $\nabla^2 = \partial T^2/\partial x^2 + \partial T^2/\partial y^2$-Laplace operator;
Index i-hereinafter omitted.
In accordance with [18], the diffusion coefficient adopted depends on the temperature:

$$D = D_0\exp(-Q/8,31\cdot T), \quad (4)$$

where D_0 the diffusion factor for element i of the alloy;
Q-the activation energy of element i in the alloy (Table 1).
The mass flux density of the i-th alloying element on the wall of the keyhole is determined by the sum of the flux densities due to evaporation (J_{ev}) and condensation (J_c):

$$J = J_{ev} + J_c. \quad (5)$$

Table 1. Components of the characteristics of the diffusion coefficient for the alloy components 5056 [18]

Components of the diffusion coefficient for alloy steel components		
Components of the diffusion coefficient	Basic alloying elements in the alloy components 5056	
	Al (liquid/solid)	Mg (liquid/solid)
D_0, m^2/s	$0.1 \cdot 10^{-5}$ / $17 \cdot 10^{-5}$	$9.9 \cdot 10^{-5}$/ $1 \cdot 10^{-4}$
Q, kJ/mol	128.0 / 143.0	71.6 / 130.0

The flux density due to evaporation J_{ev} is directly proportional to the concentration of impurities:

$$J_{ev} = J_0 \left(S/S_0\right), \quad (6)$$

where J_0 is the evaporation flux density for the pure i-th element;
S_0 and S are the initial and actual concentrations of element i in the alloy, the latter is determined by solving equation (3).
In turn, the diffusion flux density for the evaporation of element i is determined according to [14] from the formula:

$$J_0 = \mu \cdot J_v = \mu \cdot A \cdot \left(P(T)/\sqrt{\mu \cdot T}\right), \quad (7)$$

where μ is the mass of element i of the alloy in moles; J_v is the mole flow of element i of the alloy; A is a dimension factor; P(T) is the pressure of element i of the alloy under the melt.
At thermodynamic calculations the content of each chemical element C_i in vapor-gas phase of penetration channel was determined on the basis of the chemical composition of metal sample (Table 2) according to the equation [19, 20].

Table 2. Thermal characteristics of alloy components 5056

Data used for the calculation for EBW of alloy components 5056	liquid phase	solid phase
Density ρ, (kg/m^3)	2490	2640
Thermal conductivity (W/(m·K))	110	155
Heat capacity at constant pressure (kJ/(kg·K))	1, 050	0, 922
Temperature (K)	911	783
The initial concentration of elements in the alloy prior to welding, %	Al=93.6	Mg=5.84

The flux density is nonuniform evaporation on the surface of the keyhole and is proportional to the concentration of the element. Assuming complete mixing of the keyhole mixture in the flow keyhole density take on the condensation wall constant. We introduce the condensation coefficient k ($0 < k < 1$ for saturated steam k=1).

$$k \cdot \int j_{ev}\, dS = J_c \cdot S_{keyhole} \quad (8)$$

where $S_{keyhole}$-it's area keyhole; dS-elementary surface area of the keyhole.
Then, the flux density of the condensing vapor phase on the keyhole wall J_c, propor-

tional to the average concentration of elements in the pairs:

$$J_c = J_0 \cdot k \cdot \langle S \rangle / S \quad (9)$$

where and <S> is the average concentration of element i of the alloy on the surface of the keyhole.

Thus, the problem reduces to the simultaneous solution of equations (1-3) and ensure the balance of the total mass flux on the walls of the vapor-gas channel ΣJ mass flux carried away through its outlet section (condition (10) in conjunction with (11)):

$$\sum_{i=1}^{N} (J_{ev} + J_c) \cdot S_{keyhole} = \frac{\partial m}{\partial t}, \quad (10)$$

where $S_{keyhole}$ is the cross-sectional area of the keyhole and $\partial m/\partial t$ is the mass flow of metal vapour entrained by the keyhole outlet section. This mass flow is determined from the condition at the output of the keyhole for the local speed of sound [14]:

$$\frac{dm}{dt} = \sqrt{\gamma P_k \rho_k} \left(\frac{2}{\gamma + 1} \right)^{\frac{1+\gamma}{2(\gamma-1)}} \cdot S_{keyhole} \quad (11)$$

where γ is the adiabatic index and P_k and ρ_k are the vapour pressure and density in the critical section at the exit of the keyhole, respectively [20].

The system of differential equations is written as follows. The boundary conditions at the inlet boundary are constant concentration S_i (x=0, L; y)=$S0_i$ and temperature T (x=0, L; y)=T_b. At the outflow boundary, the condition for constant heat flux density is:

$$\partial^2 T / \partial x^2 \, (x = L, y) = 0. \quad (12)$$

and the mass flow density

$$\partial^2 S_i / \partial x^2 \, (x = L, y) = 0 \quad (13)$$

lateral boundary 2 and symmetry axis (y=0) are adiabatic and closed, they are given zero values of the heat flux

$$\partial T(x, y = H) / \partial y = 0 \; ; \frac{\partial T}{\partial y} = 0 \quad (14)$$

mass flow and density, respectively,

$$\partial S(x, y = H) / \partial y = 0; \frac{\partial S}{\partial y} = 0. \quad (15)$$

The surface of the keyhole (border 5) adopted by the isothermal, with a given mass flux density.

$$T = T_{\Pi}, D \frac{\partial S}{\partial x} = J. \quad (16)$$

To solve the problem of heat and mass transfer, including the transport equation of momentum, energy, mass, unused package Comsol Multiphysics. One of the input parameters of the model is the wall temperature vapor-gas channel. For each value of the parameter of the solution of the adjoint system of equations describing evaporation, condensation, diffusion, heat and mass transfer, determined by the concentration of alloying elements in the melt, pressure and concentration of chemical elements in pairs, determined by the temperature field, concentration and velocity.

Results

The numerical investigation of the evaporation processes for chemical elements on the walls of the keyhole, the condensation processes of the elements on the keyhole

walls and the diffusion of the elements in the melt was carried out with H=1.5 $\cdot 10^{-3}$ m, L=$3 \cdot 10^{-3}$ m, r=$2.5 \cdot 10^{-4}$ m and l=$1.6 \cdot 10^{-3}$ m. The data used are shown in Table 2. For the calculation of the task used mesh refinement in all the estimated volume of the body.

Fig. 2 shows the results of calculations of concentration of chemical elements in the liquid and the solidified keyhole portion along the weld.

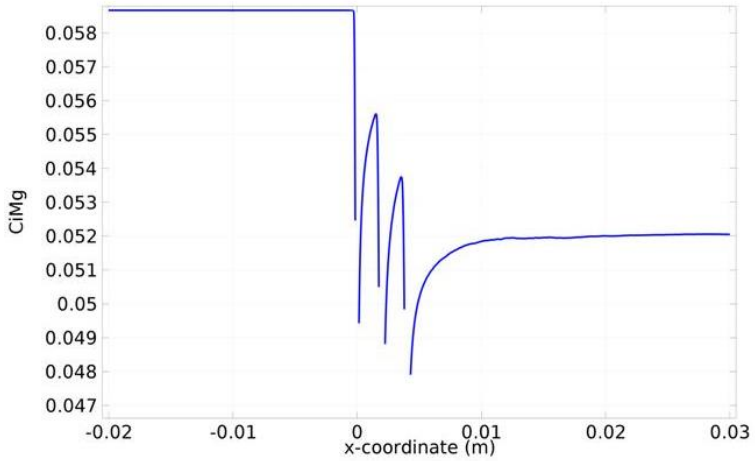

Fig. 2. Calculated values of changes in the concentration of Mg along the seam weld The length of the computational domain (the axis 0X), m

The graph in Fig.2 can be divided into four areas along the x-axis. The first area being from-0.02 to 0 m is the base metal. The second area being from 0 to 0.004 m is responsible for the vaporization processes. The liquid weld pool exists in the third area being from 0.004 to 0.01 m. And the solid welded joint is in the fourth area. In the second area, where the keyhole exist, the concentration of magnesium decreases from 0.058 to 0.048 relative units (rel. un.), this is caused by an intensive evaporation process. Then in the weld pool the concentration of magnesium increases due to the diffusion processes in the liquid, but magnesium concentration planes in the solid phase and becomes equal to 0.052 rel. un.

The aim of the experimental procedure was to determine the temperature in the keyhole during EBW according to the chemical composition of the vapour formed over the welding zone. For the guarantee of high speed of electron beam deviation at the dynamic positioning the deflectors of an electron gun were connected to the broadband current amplifier having the top limit of the pass band being equal to 200 kHz. The signals were input through the digital-to-analogue interface from the computer system to the ports of these amplifiers, the system being functioned under the developed program which provided given space-time characteristics of the heat interaction on the specimens.

The weld parameters (welding speed, energy distribution in the beam, the distance

between dynamically positioned beams) have been varied in accordance to the matrix of the planning an experiment.
The resulting coating was analysed using roentgen fluorescence, performed on mode of 6 (Table. 3). The data obtained are presented in Table 4 ang Fig.3.

Table 3: Parameters modes EBW

Number Weld	Welding current, mA	The distance between the beams, mm	Welding speed, mm / sec	The energy distribution (ms)
6	40	4 мм	5	1:2:1 (40:80:40)

Table 4: The data obtained

№	Al, rel. un.	Mg, rel.un.
1	0, 948	0, 0440
2	0, 935	0, 0515
3	0, 934	0, 0572
4	0, 933	0, 0584
The average value of the concentration		
	0, 937	0, 0528
The concentrations of the reference data		
	0, 911-0, 9368	0, 058-0, 068

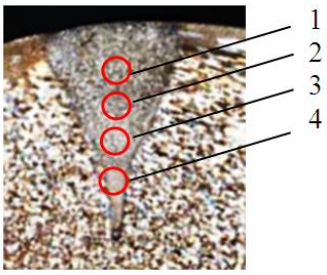

Fig. 3. The welded joint obtained by EBW dynamic splitting of the electron beam; 1-4-zone determination of chemical composition

Roentgen fluorescent analysis of the cross-section of the penetration area obtained during the operation 6 shows the significant depletion of the volatile component of the alloy (Mg) to 0.044 rel. un. in the top part of the joint. Magnesium concentration increases to the root part of the joint and reaches the acceptable values being 0.058-0.068 rel. un. Consequently mean value of magnesium concentration in the welded joint is 0.0528 rel. un., which is in accordance with the mean value of magnesium concentration obtained at the process simulation (0.052 rel. un.).
The developed simulator describes heat-and-mass transfer during EBW with the dy-

namic positioning of electron beam and allows to predict the chemical composition of welded joints at EBW. Verification of the simulator has been carried out by the comparing with the results of the chemical analysis of the welded metal penetration areas.

Acknowledgements
This work was supported by a grant from the Russian Foundation for Basic Research 14-08-96008 ural_a and with financial support for the initial base part of the state task (No. 1201460538).

References:

[1] Wichmann V.B. Kozlov A.N., Maslov M.A. Advantages and disadvantages of the electron beam during welding compared to Laer and arc // Reports of III Saint Peterburskoy Intern. scientific. prac. Conf., June 24-26 2014goda. SPb.: Publishing House of the Polytechnic. University Press, 2014. C.4-19.

[2] Ol'shanskaya T.V., Trushnikov D.N., Belenky V.J., Mladenov G.M. Effect of oscillation of the electron beam on the structure and properties of the weld // Welding production. 2012. № 11. C. 13-18.

[3] Rüthrich K., Zenker R., Mangler M. Investigations Relating to Electron Beam Multipool Welding of Metal Welds Based on Cast Iron, In: 64th Annual Assembly and International Conference of the International Institute of Welding, Chennai (Indien), 17.-22.07.2011, Proceedings (CD, paper IC95).

[4] Zenker R. Modern Thermal Electron Beam Processes-Research Results and Industrial Application // La Metallurgia Italiana. Aprile 2009. pp. 1-8.

[5] Mladenov G.M. Electron beam welding: monograph / G.M. Mladenov, D.N. Trushnikov, V.Y. Belenky, E.G. Koleva.-Perm: Publishing house of Perm. nat. Issled. Polytechnic. University Press, 2014.-374 p.

[6] Mupaveva T.P., Dpagunov V.K., Plum A.P. Gonchapov A.L. Features and properties of the structure to the welded joints of steel plates made by electron-beam welding // Welding production. 2010. № 6. C. 38-42.

[7] A.F. H. Kaplan, P. Norman and I. Eriksson: Analysis of the keyhole and weld pool dynamics by imaging evaluation and photodiode monitoring, Proceedings of LAMP2009-the 5th International Congress on Laser Advanced Materials Processing, (2009) 1-6.

[8] Askar'yan G.A., Morozov E.M. The pressure of the evaporation of the substance in the beam-radiation // Journal of Experimental and Theoretical Physics. 962. T.43. Vol. 6. S. 2319-2320.

[9] W.-I. Cho, S.-J. Na, C. Thomy, F. Vollertsen Numerical simulation of molten pool dynamics in high power disk laser welding // Journal of Materials Processing Technology, 212 (2012). 262-275.

[10] Sudnik W., Erofeew W., Radaj D., Breitschwerdt S.Numerical simulation of weld pool geometry in laser beam welding // Journal of Physics D: Applied Physics. 2000. T. 33. № 6. S. 662-671.

[11] Yazovskih V.M., V.V. Utochkin Thermodynamic evaluation of the evaporation temperature due to the pressure of steam in the channel penetration in electron beam welding // Physics and Chemistry of Materials Processing. 1977. № 2. S. 73.

[12] Lebedev B.D. The calculations in the theory of welding processes: to teach. Allowance.-K.: SMC IN, 1992.-320 p.

[13] Turichin G.A., Cybulski I.A., Kuznetsov M.V., Solmonov V.V. Valdaytseva E.A. Simulation of the dynamic behavior of the weld pool during laser and hybrid welding with deep penetration // Scientific and technical statements STU. 2010. № 110. S. 175-181.

[14] BY R. Ray, T.A. Palmer, J.W. Elmer, and T. Debroy Heat Transfer and Fluid Flow during Electron Beam Welding of 304L Stainless Steel Alloy // Welding Journal. Mach 2009, VOL. 88. P. 54-s-61-s.

[15] V.A. Lopota, Turichin G.A., Valdaytseva E.A., Malkin P.E., Gumenyuk A.V. Computer system simulation of electron beam and laser welding // Automatic welding. 2006. № 4. S. 36-39.

[16] Sudnik V.A. Section "Fundamentals of the welding simulation" in the directory publishing AMS International (USA) // Welding production. 2015. №. S. 23-26.

[17] Dilthey U., Goumeniouk A., Lopota V., Turichin G., Valdaitseva E. Development of a theory for alloying element losses during laser beam welding // journal of physics d: applied physics. 2001 m. 34. № 1. pp. 81-86.

[18] Yong Du et al. Diffusion coefficients of some solutes in fcc and liquid Al: critical evaluation and correlation // Materials Science and Engineering. A363 (2003). pp. 140-151.

[19] Salomatova E.S. Trushnikov D.N., Belenky V.J. Simulation temperature vapor gas passage under electron beam welding // Thermal processes in the art. 2013. №11. Pp 514-519.

[20] D.N. Trushnikov, E.S. Salomatova, V.Y. Belenky, W. Rayzgen estimate of the temperature in the channel penetration in electron beam welding // Welding production. 2015. № 2. pp 18-22.